Journal of Power Sources 180 (2008) 440–451

Contents lists available at ScienceDirect

Journal of Power Sources

journal homepage: www.elsevier.com/locate/jpowsour

Understanding cathode flooding and dry-out for water management in air breathing PEM fuel cells

Mathieu Paquin, Luc G. Fréchette*

Université de Sherbrooke, Department of Mechanical Engineering, 2500 Boul. Université, Sherbrooke, Québec J1K 2R1, Canada

ARTICLE INFO

Article history:
Received 15 January 2008
Received in revised form 6 February 2008
Accepted 6 February 2008
Available online 16 February 2008

Keywords:
PEMFC
Free convection
Air breathing
Water management
Dry-out
Flooding

ABSTRACT

An analysis of water management in air breathing small polymer electrolyte membrane fuel cells (PEMFCs) is presented. Comprehensive understanding of flooding and dry-out limiting phenomena is presented through a combination of analytical modeling and experimental investigations using a small PEMFC prototype. Configurations of the fuel cell with different heat and mass transfer properties are experimentally evaluated to assess the impact of thermal resistance and mass transport resistance on water balance. Manifestation of dry-out and flooding problems, as limiting phenomena, are explained through a ratio between these two resistances. Main conclusions are that decreasing the ratio between thermal and mass transport resistance under a certain point leads to flooding problems in air breathing PEMFC. Increasing this ratio leads to dry-out of the polymer electrolyte membrane. However, too high thermal resistance or too low mass transport resistance reduces the limiting current by pushing forward the dry-out problem. This work provides a framework to achieve the proper balance between thermal rejection and mass transport to optimize the maximum current density of free convection fuel cells.

1. Introduction

One of the main problems in the development and commercialisation of micro polymer electrolyte membrane fuel cells (PEMFCs) as small power sources (<10 W) resides in the miniaturisation of auxiliary components that must be scaled down with the stack. External subsystems, such as the blower, humidification unit and heat exchanger, increase the complexity for balance of the plant of the fuel cell system and typically have low efficiencies and power density when miniaturised. This suggests that micro-PEMFC [1–4] may not lead to viable power sources unless research is done on miniature balance of plant components or passive approaches are developed.

Running PEMFCs in free convection mode significantly reduces the number of subsystems required. Absence of direct control over the air stream in the PEMFC makes temperature and humidity control an important problem. In fact, air breathing fuel cells consistently achieve lower performance than cells operated under forced convection mode. Many studies have been conducted on fuel cells running in free convection mode, either through modeling or experimentation [5–19]. Main conclusions are that in this operation mode, problems limiting performances are due to mass transport and water management. Also, the importance of the surrounding conditions is highlighted [7,8,13].

Mennola et al. [14] concluded that for cell temperatures below 40 °C, the limiting problem was the system's inability to remove water. Modroukas et al. [15,16] conducted a study of air breathing PEMFC running at low temperature (20–30 °C). Under these operating conditions, the limiting factor was also water accumulation which caused flooding of the cell. To increase cell performance, utilisation of a passive water control system based on hydrophilic material that enhances water removal from the cell was demonstrated. O'Hayre et al. [17] ran a free convection cell under temperatures ranging from 10 to 80 °C and demonstrated the dependence of performance on humidification of the cell. At temperatures higher than 70 °C, membrane dry-out was found to be the limiting phenomenon. Morner and Klein [18] also concluded that membrane humidity is one of the most significant factors in determining fuel cell performances in free convection mode. Jeong et al. [8] also concluded that the performances of air breathing fuel cells are strongly dependant on water management.

This past work highlighted two interesting points. First, water management problems seem to be the limiting phenomena, either by flooding the cathode domain or by dry-out of the electrolyte. Second, the operating temperature is important in defining the limiting problem. Running in free convection mode implies a strong dependency between heat transfer, mass transfer and temperature of the system. Packaging dimensions and material properties are then of considerable importance, especially for fuel cell systems without air flow and temperature control, such as portable air breathing products.

* Corresponding author. Tel.: +1 819 821 8000x62799.
E-mail address: Luc.Frechette@Usherbrooke.ca (L.G. Fréchette).

0378-7753/$ – see front matter © 2008 Elsevier B.V. All rights reserved.
doi:10.1016/j.jpowsour.2008.02.012

Nomenclature

C_p	specific heat ($J\,kg^{-1}\,K^{-1}$)
D	diffusion coefficient ($m^2\,s^{-1}$)
E_{OCV}	reference reversible fuel cell voltage
F	Faraday's constant (96,487 $C\,mol^{-1}$)
g	gravity constant (9.8 $m\,s^{-2}$)
$\Delta\bar{g}_f$	Gibbs free energy change
h	free convection heat or mass transfer coefficient ($W\,m^{-2}\,K^{-1}$) or ($m\,s^{-1}$)
H_{fg}	heat of water condensation (40 $kJ\,mol^{-1}$)
I	current density ($A\,m^{-2}$)
I_0	exchange current density ($A\,m^{-2}$)
I_l	limiting current density ($A\,m^{-2}$)
$I_{l\text{-}max}$	maximum limiting current density ($A\,m^{-2}$)
$I_{l\text{-}ideal}$	ideal limiting current density ($A\,m^{-2}$)
k	thermal conductivity ($W\,m^{-1}\,K^{-1}$)
L	characteristic length for heat and mass transfer
$\dot{m}$	mass flow ($kg\,s^{-1}$)
M	molar weight ($g\,mol^{-1}$)
N	molar flux ($mol\,s^{-1}\,m^{-2}$)
Q	heat (W)
$\dot{Q}_G$	heat generated by fuel cell (W)
R	universal gas constant (8.314 $J\,mol^{-1}\,K$)
$R_{electric}$	fuel cell electrical resistance (Ω)
R_{ionic}	fuel cell ionic resistance (Ω)
RH	relative humidity
S	surface (m^2)
T	temperature (K)
w	mass fraction
W_{GDL}	GDL thickness (m)
x	molar fraction

Greek letters

α_{cell}	charge transfer coefficient
$\delta_{membrane}$	Nafion® membrane thickness (m)
ε	porosity
σ_{RH}	membrane conductivity ($\Omega^{-1}\,m^{-1}$)

Subscripts

a	active area
c	cathode
cell	fuel cell
cr	critical
GDL	gas diffusion layer
m	mass transport
packaging	cell subsystems excluding cathode and GDL
s	GDL interface with environment
T	thermal
α	species: N_2, O_2, H_20
β	species: N_2, O_2, H_20
∞	environment

In this paper, we develop a simple one-dimensional model of a free convection PEMFC with a planar configuration that integrates heat and mass transfer. This model will be validated experimentally and then used along with other experimental results to analyse the impact of thermal resistance and mass transport resistance. To do so various configurations of the prototype with different heat and mass transfer properties will be evaluated experimentally. The manifestation of dry-out and flooding as limiting phenomena will be presented in term of ratio between heat and mass transfer. This work unifies diverging conclusions from previous work [14–17] on the manifestation of the limiting problems. Also, the importance of the system's packaging will be highlighted and experimentally shown.

2. Free convection planar PEMFC model

2.1. Free convection heat and mass transfer coefficient

Free convection on exposed surfaces of a planar PEMFC is characterized by heat and mass transfer resulting from the electrochemical reaction in the cell. Oxygen consumption and water production, resulting from cell operation, will generate concentrations gradients and density changes in the air. Heat loss from the cell creates a temperature gradient which generates a density variation in the air surrounding the cell and creates convection. All these gradients will cause heat and mass transfer between the cell and its environment. An exact free convection model should consider both heat and mass transfer phenomena combined. But, as a first approximation, heat transfer and mass transfer will be considered separately, related by the heat and mass transfer analogy. In this section, the heat transfer coefficient ($\bar{h}_T$) and air species mass transfer coefficient ($\bar{h}_m^{\alpha}$) will therefore be determined using empirical correlations.

Natural convection heat transfer can be described by the non-dimensional heat transfer coefficient, referred to as the Nusselt number (Nu_L). For natural convection driven by heat transfer only, empirical correlations depending on geometries and boundary conditions express the Nusselt number as a function of the Grashof (Gr_L) and Prandtl (Pr) non-dimensional numbers [20]:

$$\overline{Nu}_L = \frac{\bar{h}_T k_{air}}{L} = f(Gr_L, Pr) \tag{1}$$

Free convection from a planar PEMFC will simply be represented as a vertical heated plate. For this situation, the heat transfer correlation is [20]:

$$\overline{Nu}_L = 0.54(Gr_L\,Pr)^{1/4}, \quad \text{for } 10^4 \le Gr_L\,Pr \le 10^7 \tag{2}$$

$$Gr_L\,Pr = Ra_L = \frac{g\beta(T_s - T_\infty)L^3}{\nu\alpha} \tag{3}$$

As presented in Eqs. (2) and (3), only the temperature gradient is considered to lead to a density change in the air. Species concentration variation will also induce density gradient, but this effect is not considered here for simplicity. As presented by O'Hayre et al. [17], the thermal gradient is the main factor in natural convection of air breathing PEMFC and accounts for about 75% of the density gradient. This approximation leads to an underestimated value of the heat transfer coefficient.

The Sherwood (Sh_L) non-dimensional number can be used to describe free convection mass transfer. This number can be empirically correlated, depending on geometries and boundary conditions, with the non-dimensional Grashof (Gr_L) and Schmidt (Sc) numbers:

$$\overline{Sh}_L^{\alpha} = \frac{\bar{h}_m^{\alpha} D_{air-\alpha}}{L} = f(Gr_L, Sc_\alpha) \tag{4}$$

In order to use the analogy between heat and mass transfer for a fluid flows where there is simultaneous heat and mass transfer, the Lewis (Le) number, which is the ratio between heat and mass diffusivity, should be close to unity. For diffusion of oxygen and water vapour in ambient air at 25 °C, the Lewis number is

$$Le_{O_2} = \frac{Sc_{O_2}}{Pr} = 1.04 \tag{5}$$

$$Le_{H_2O} = \frac{Sc_{H_2O}}{Pr} = 0.82 \tag{6}$$

Considering that the Lewis number values are near unity, the analogy between heat and mass transfer will be used here. An equation for each air species (N_2, O_2, H_2O) can then be obtained

$$\overline{Sh}_L^{\alpha} = 0.54(Gr_L^{\alpha}\, Sc_{\alpha})^{1/4}, \quad \text{for } 10^4 \le Gr_L^{\alpha}\, Sc_{\alpha} \le 10^7 \tag{7}$$

The term $Gr_L\, Sc_\alpha$ from Eq. (7) is calculated using a relation proposed by Li et al. [9]:

$$Gr_L^{\alpha}\, Sc_{\alpha} = Ra_L^{\alpha} = \frac{g\gamma_{\alpha}(w_{\alpha\text{-s}} - w_{\alpha\text{-}\infty})L^3}{\nu D_{\text{air}-\alpha}} \tag{8}$$

where

$$\gamma_{\alpha} = \frac{M_{\text{air}} - M_{\alpha}}{w_{\alpha}M_{\text{air}} + ((1 - w_{\alpha})M_{\alpha})} \tag{9}$$

Knowing the mean value of Nu_L and Sh_L, it is possible to calculate the mean value of the heat and mass transfer coefficients:

$$\bar{h}_{\text{T}} = \frac{0.54(Gr_L\, Pr)^{1/4}k_{\text{air}}}{L} \tag{10}$$

$$\bar{h}_{\text{m}}^{\alpha} = \frac{0.54(Gr_L^{\alpha}\, Sc_{\alpha})^{1/4}D_{\text{air}-\alpha}}{L} \tag{11}$$

2.2. Model scope and assumptions

The scope of the model is to identify the manifestation of limiting problems at the cathode of an air breathing PEMFC; either water management problems or mass transport limitations. Qualitative results that show dominant physics are expected, as opposed to precise predictive results. This model is inspired of those presented by Refs. [11,12,14,15,17,19]. The main assumptions used to develop the model are

- one-dimensional;
- steady state;
- dry hydrogen at the anode;
- no water crossing the membrane to the anode;
- uniform activity over the cathode surface;
- infinitely thin cathode;
- driving force for mass transport in the gas diffusion layer is by diffusion only [15];
- uniform water content across the Nafion® membrane;
- equilibrium between relative humidity at the cathode and water activity in the membrane.

An important assumption of the model is the absence of saturation effects due to water condensation within the gas diffusion layer and in the catalyst region. Modroukas [15] showed the importance of this aspect to model a free convection PEMFC running under free convection at low temperature. Under these conditions water accumulation is the dominant problem that causes cell failure. Since the focus here is to identify if flooding will occur and not to predict the performance once it has, the model does not include the effect of water accumulation. Therefore, the model will not include the impact of relative humidity (RH) going over 100% and subsequent water formation that would impede oxygen diffusion to the catalyst region. The important aspect that will be captured is when the water partial pressure is higher than the water saturation pressure, to identify when water will condense in the cathode and flooding will occur. To appropriately do so, heat of water condensation (H_{fg}) will be taken in account as heat generated by the cell.

Another impact of the assumptions presented above is related to water content in the Nafion® membrane. The last two assumptions listed above imply that water conditions within the membrane will be fixed by the temperature and partial pressure of water at the interface between the cathode and the GDL. This assumption limits the predictive accuracy of the model but captures the tendency for membrane water content and its related ionic conductivity. Water absorption, desorption and transport in the Nafion® membrane [21,22] are not consider here. Future work should consider water transport in the entire membrane electrode assembly (MEA), including water balance at the anode.

2.3. Model domains

A control volume approach is used to consider energy and mass balance. The model is divided in three domains. The first domain is the GDL which goes from cathode's catalyst region to the interface of the GDL with the environment. At the interface of the catalyst with the GDL, the boundary conditions represent the electrochemical reactions occurring in the cell, namely: heat generation ($\dot{Q}_{\text{G}}$), water production (N_{H_2O}) and oxygen consumption (N_{O_2}). These fluxes are directly related to the cell current density (I). The second domain is the GDL interface with the environment. Boundary conditions for this domain are environment species molar fraction ($x_{\infty\text{-}\alpha}$) and temperature (T_∞). The third domain represents rest of the fuel cell, such as the packaging, that can exchange heat with the environment at T_∞; mass transport only occurs in domains 1 and 2. The presence of this third domain is important considering the analysis presented here, which includes the packaging of the system and not only the cathode and the GDL. The diagram in Fig. 1 presents heat and mass transfer fluxes and sketches the trends of species molar fraction and temperature within the domains.

In the GDL, heat transfer is modeled as conduction only (Q_{c}). Mass transfer occurs via species diffusion through the porous media. The governing equation for the displacement of oxygen, water vapour and nitrogen is given by the Maxwell–Stefan diffusion equation for multi-component systems [23].

$$Q_{\text{C}} = -k_{\text{GDL}}S_{\text{a}}\frac{T_{\text{s}} - T_{\text{c}}}{W_{\text{GDL}}} \tag{12}$$

$$\sum_{\beta=O_2,H_2O,N_2} \frac{RT_{\text{c}}}{PD_{(\alpha-\beta)\text{\_eff}}}(x_{\beta}N_{\alpha} - x_{\alpha}N_{\beta}) = -\nabla x_{\alpha}, \quad \text{for } \alpha = O_2,\ H_2O,\ N_2 \tag{13}$$

Binary diffusion coefficients of species ($D_{\alpha\text{-}\beta}$) are calculated using relations from Bird [23]. In order to take into account porous media effects, the Bruggemann correction factor is used to correct the binary diffusion coefficients for GDL porosity (ε_{GDL}) [14].

$$D_{\alpha-\beta} = \frac{a}{P}\left(\frac{T}{\sqrt{T_{\text{cr}\alpha}T_{\text{cr}\beta}}}\right)^{b}(p_{\text{cr}\alpha}p_{\text{cr}\beta})^{1/3}(T_{\text{cr}\alpha}T_{\text{cr}\beta})^{5/12}\sqrt{\frac{1}{M_{\alpha}} + \frac{1}{M_{\beta}}} \tag{14}$$

$$D_{(\alpha-\beta)\text{\_eff}} = \varepsilon_{\text{GDL}}^{3/2}D_{\alpha-\beta} \tag{15}$$

On the exposed surface of the GDL, heat and mass transfer are driven by free convection. Mean values of heat and mass transfer coefficients ($\bar{h}_{\text{T}}$ and $\bar{h}_{\text{m}}^{\alpha}$) are used. The following are the governing equations that link heat rejection and species movement on the GDL surface:

$$Q_{\text{C}} = \bar{h}_{\text{T}}S_{\text{a}}(T_{\text{s}} - T_{\infty}) \tag{16}$$

$$\sum_{\beta=O_2,H_2O,N_2}(x_{\beta}N_{\alpha} - x_{\alpha}N_{\beta}) = -\Delta x_{\alpha}\frac{P}{RT_{\text{s}}}\bar{h}_{\text{m}}^{\alpha} \tag{17}$$

An important value pictured on Fig. 1 is Q_{out}, which accounts for all other heat loss mechanisms in the system except that from the GDL surface (Q_{c}). A significant part (≈90%) of the heat generated by the fuel cells will be rejected in the environment through the

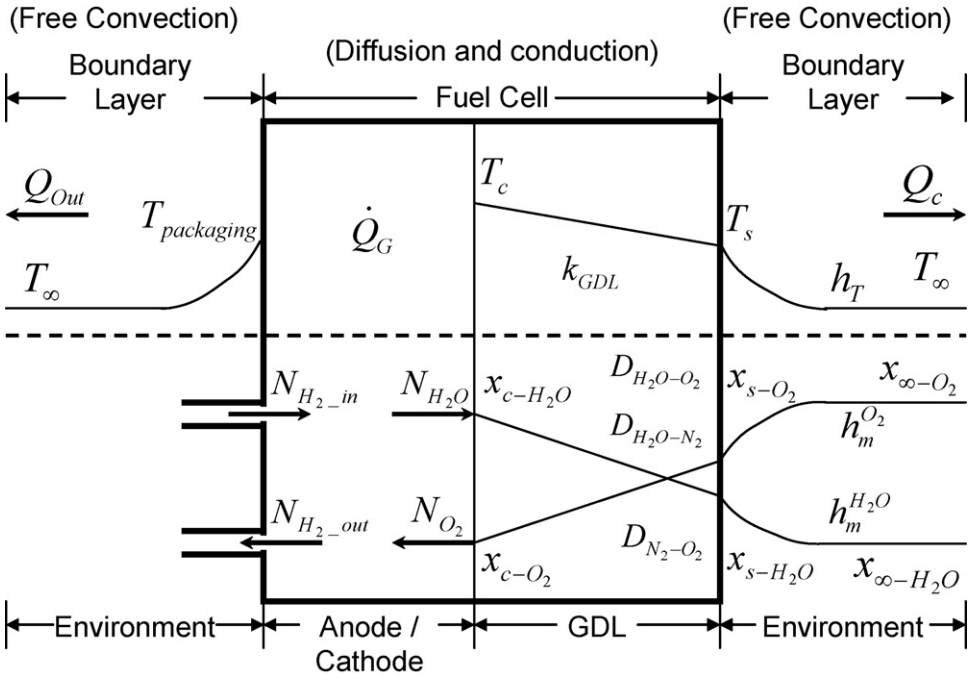

Fig. 1. Domains for the free convection planar PEMFC model with heat transfer (top) and mass transfer (bottom) phenomena. The free convection transfer processes at the cathode are depicted on the right hand side, while the other transfer processes for the anode and the rest of the packaging are shown on the left.

rest of the system (packaging) in contact with the environment and through heating of the system's hydrogen supply (Q_{out}).

$$Q_{out} = (A_{cell} - S_A)h_{T\_packaging}(T_{packaging} - T_\infty) + \dot{m}_{H_2}C_p(T_c - T_\infty) \quad (18)$$

2.4. Relation between heat and mass transfer and the electrochemical reactions

A fundamental part of the model is to gather heat and mass transfer physics with the electrochemical reaction that occurs within the cell. Environment conditions combined with heat generated and mass fluxes are the input necessary to establish temperature and species partial pressure of the cell for an operation point. These last two inputs are driven by the electrochemical reaction of the cell [24].

Using the stoichiometry of the reaction, it is possible to establish the following molar flux for oxygen consumption and water vapour generation.

$$N_{O_2} = \frac{-I}{4F} \quad (19)$$

$$N_{H_2O} = \frac{I}{2F} \quad (20)$$

In order to describe the fuel cell polarization curve (V–I curve), voltage drop must be determined. There are three main sources of voltage drop: reaction kinetics (η_K), Ohm's law (η_{IR}) and mass transport (η_{MT}). Voltage drop from reaction kinetics can be described by the *Tafel* equation [24]:

$$\eta_K = \frac{RT_c}{2\alpha_{cell}F}\ln\left(\frac{I}{I_0}\right) \quad (21)$$

where I_0 is the exchange current density and α_{cell} is the charge transfer coefficient. These values will be fitting parameters in the model. Voltage drop from Ohm's law is due to internal electrical resistance and ionic resistance of the Nafion® membrane. Electrical resistance is mainly due to contact resistance between components and the material's internal resistance. Ionic resistance is mainly related to the electrolyte membrane thickness, water content and temperature. The ionic conductivity dependency with water content of the membrane will be estimate using an empirical relation developed by Sone et al. [25], which relates ionic conductivity of Nafion® with relative humidity.

$$\eta_{IR} = IS_a(R_{electric} + R_{ionique}) \quad (22)$$

$$R_{ionique} = \frac{\delta_{membrane}}{S_a\sigma_{RH}} \quad (23)$$

$$\sigma_{RH} = 7.46x^3 - 7.45x^2 + 3.13x - 0.378 \quad (24)$$

where x is the relative humidity. As presented in the assumptions, this value will be approximate by relative humidity at the cathode (RH_C) because equilibrium is considered between the relative humidity at the cathode and the water activity in the membrane. Also, Eq. (24) is accurate only for a temperature of 30 °C. As presented in Ref. [25] ionic conductivity of a Nafion® membrane not only depends on its configuration and relative humidity but also on its temperature.

$$RH_C = \frac{X_{c\text{-}H_2O\_(gas)}P}{P_{saturation,H_2O}} \quad (25)$$

Using saturation pressure values from Van Wylen et al. [26], a third order polynomial function was defined to fit saturation pressures between 15 and 70 °C.

$$P_{saturation,H_2O} = 0.164T_c^3 + 145.32T_c^2 + 43023.33T_c - 4263759.49 \quad (26)$$

Voltage drop due to mass transport comes from the decrease in oxygen partial pressure at the catalyst surface [24].

$$\eta_{MT} = \frac{-RT_c}{4F}\ln\left(\frac{x_{O_2\text{-}c}}{x_{O_2\text{-}\infty}}\right) \quad (27)$$

It is possible to write the polarization value of the fuel cell as follows [11]:

$$V = E_{OCV} - \eta_K - \eta_{IR} - \eta_{TM} \tag{28}$$

where E_{OCV} is the fuel cell open circuit voltage [24].

$$E_0 = \frac{-\Delta \bar{g}_f}{2F} \tag{29}$$

System loss will result in heat generation ($\dot{Q}_G$) proportional to voltage drop (η_K, η_{IR} and η_{TM}). We consider that water is produced in vapour form, so to be thermally consistent; we calculate E_0 using lower heating value (LHV) of the Gibbs free energy variation ($\Delta \bar{g}_f$). Heat released during water condensation inside the cell is accounted for using heat of water condensation (H_{fg}). The heat generation rate can be expressed as

$$\dot{Q}_G = IS_a \left(E_0 - V + \frac{H_{fg} x_{c\text{-}H_2O\_liquid}}{2F} \right) \tag{30}$$

If $RH_C < 100\%$, then the molar fraction of liquid water at the cathode is $x_{c\text{-}H_2O\_liquid} = 0$, otherwise $x_{c\text{-}H_2O\_liquid}$ is calculated using saturated value of water molar fraction ($x_{c\text{-}H_2O\ (saturated)}$):

$$x_{c\text{-}H_2O\_liquid} = x_{c\text{-}H_2O} - x_{c\text{-}H_2O\ (saturated)} \tag{31}$$

Using the equations developed above, an iterative approach can be used to find a temperature value of the cell (T_c) that will match heat generated through electrochemical reactions ($\dot{Q}_G$) with heat loss to the environment (Q_c and Q_{out}). To do so, an approximate value of T_c will be fixed and used to calculate the temperature at the surface of the GDL (T_s) based on conduction through the GDL and the stainless steel grid that are over the cathode. The temperature of the rest of the packaging ($T_{packaging}$) is calculated as heat conduction through a typical thickness of the fuel cell packaging. These temperatures will then be used to calculate heat transfer coefficients h_T and $h_{T\_packaging}$ with Eq. (10). Q_c and Q_{out} will then be determined using Eqs. (16) and (18). It should be noted that this simple modeling of heat loss from the system is corrected by a fitting factor (C_{heat}) that is determined from the experimental results of the baseline prototype, and used throughout. The energy balance presented in Eq. (32) is done at a specific operating point, defined by the current density (I) which also fixes oxygen and water vapour partial pressure by imposing the corresponding molar fluxes as presented in Eqs. (19) and (20). Knowing species partial pressure and an approximation of temperatures within the system, voltage loss (V) and heat generated ($\dot{Q}_G$) are calculated using Eqs. (28) and (30). Iterations will be done around T_c as long as the energy balance, Eq. (32), is not satisfied.

$$\dot{Q}_G = Q_c + Q_{out} \tag{32}$$

3. Experimental

3.1. Small PEMFC prototype

In order to validate the model, a small PEMFC was designed and fabricated. Fig. 2 presents an exploded view of the prototype with a description of the various components. External dimensions of the prototype are 3.5 cm long by 1.9 cm large and 0.635 cm thick. Active area of the cell is 2 cm^2. Table 1 summarises the values used in the analytical simulation of the prototype.

3.2. Experimental set-up and results

Tests were run using a fuel cell test station fabricated by *Fuel Cell Technologies, Inc.* Dry hydrogen was supplied to the anode using a stoichiometry ratio of 3 and atmospheric air was supplied to the cathode by free convection with the ambient. During testing, the polarization curve (V–I) was measured as well as the temperature and relative humidity of the cathode GDL's exposed surface. It is important that these measurements be made as close as possible to the GDL but geometrical limitations did not allow measurements to be taken directly on GDL's top surface. Hence, we expect the actual GDL temperature to be slightly higher than the measurement, leading to some discrepancies between results and modeling. Measurement uncertainty in current density and voltage are small, respectively ±0.003 A and ±0.003 V. For temperature and relative humidity, we evaluate the uncertainty to be respectively less than ±1 °C and ±7.5% RH, considering sensor accuracy and measurement repeatability.

Experimental results were taken in steady-state conditions except for points having a relative humidity of 100%. These operating points presented water accumulation, which mean that water flux generated by the reaction was higher than the maximum water

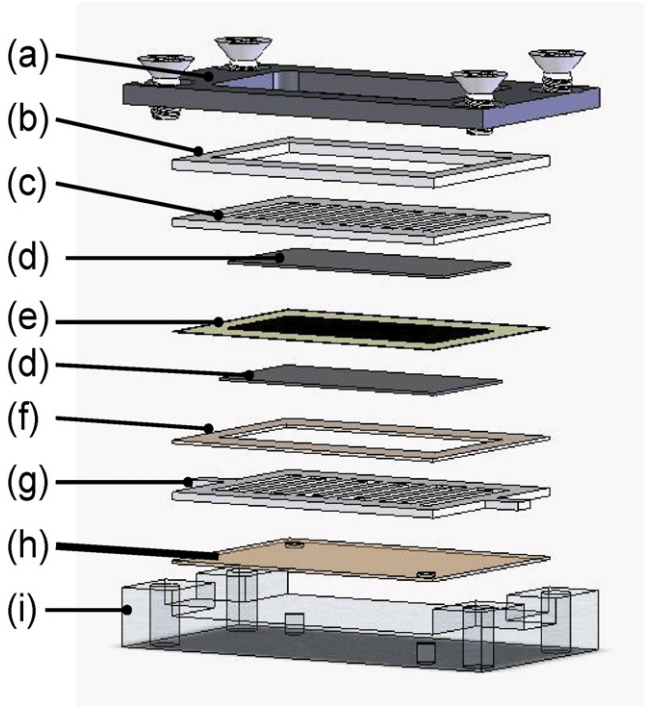

Fig. 2. Exploded view of the small PEMFC prototype. (a) Stainless steel support plate for cathode, (b) Grafoil® sheet, (c) stainless steel grid for cathode, (d) GDL (SGL Carbon 10 BB), (e) MEA: catalyst coated NAFION® NRE 212 and loading of 0.5 mg Pt cm^{-2} from Ion Power, Inc., (f) seal to prevent lateral diffusion of hydrogen in anode GDL, (g) stainless steel anode channel, (h) seal for anode flow, and (i) Plexiglass support plate for anode.

Table 1
Model input values

Model parameter	
RH_∞	As specified
T_∞	As specified
$R_{electric}$	0.2 Ω
E_{OCV}	1.185 V
W_{GDL}	0.38 mm
ε_{GDL}	0.84
S_a	2 cm^2
S_{cell}	20 cm^2
L	3.5 cm
$\delta_{membrane}$	70 μm
α_{cell}	0.22 [24]
k_{GDL}	10 $W m^{-1} K^{-1}$ [17]
Fitting parameter	
I_0	0.07 $A m^{-2}$
C_{heat}	2.17

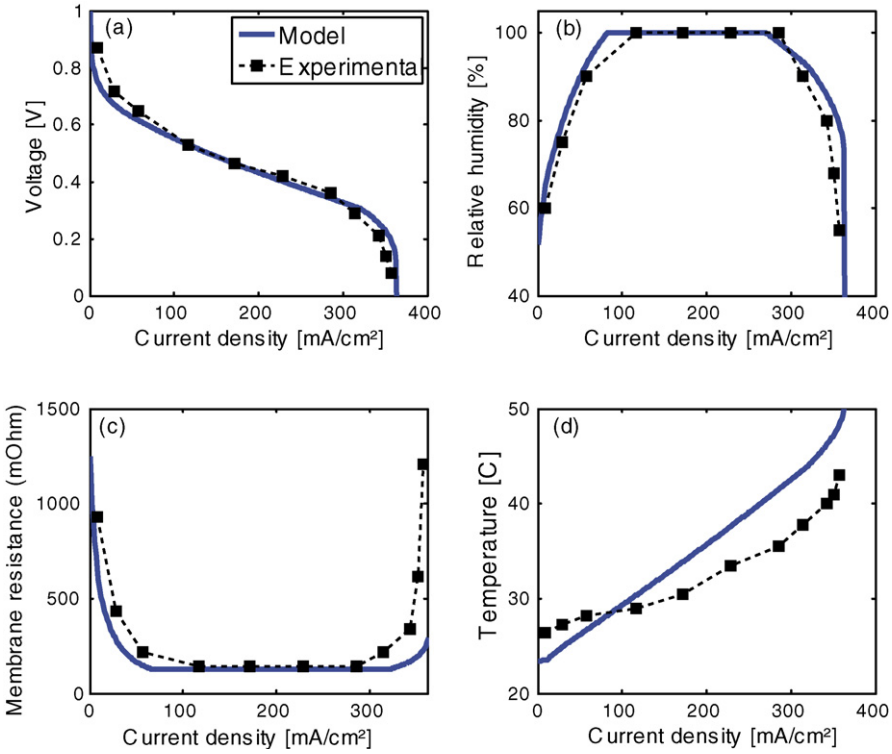

Fig. 3. Comparison between experimental and simulation results for free convection fuel cell operated at ambient air of 23.5 °C and 40% RH as a function of current density: (a) polarization curves, (b) relative humidity on surface of cathode GDL, (c) fuel cell membrane resistance calculated by Eqs. (23) and (24), based on relative humidity at the surface of the cathode GDL for the experimental results, and (d) temperature on surface of cathode GDL.

flux removed by free convection. Therefore, long-term operation under these conditions would create water accumulation at the cathode, significantly reducing oxygen diffusion and limiting the achievable current density due to mass transport resistance. Results under these conditions were taken before water accumulation, so these results are not achievable in long term, steady-state operation.

Fig. 3 presents experimental results for the small PEMFC prototype compared to results obtained with the model developed previously. The prototype limiting current density (I_l) occurs at 360 mA cm^{-2} and the maximum power density is 103 mW cm^{-2}. The four curves presented in Fig. 3 put in evidence that the limiting phenomenon is dry-out, which will be discussed in details in the following section. Both the model and experimental results show that the decrease of relative humidity at high current density, which causes ionic resistance to increase, coincides with the non-linear voltage drop that stops the reaction.

The main difference between experimental and analytical results occurs in temperature results. However, trends linking temperature, relative humidity, membrane ionic resistance and polarization curve are well captured. Considering the scope of the model, which was to demonstrate the manifestation of the problems limiting small PEMFC performance, the model is adequate.

As presented in Table 1, fitting parameters were necessary to match the model with the experimental results. I_0 is used to fit the voltage drop from reaction kinetics and C_{heat} is a heat transfer correction factor. Temperature is a commonly adjusted value in simplify model. The heat transfer correlations used here are for a highly simplified geometry, neglect radiation and density changes from concentration gradients. Thus, they are certainly not quantitatively exact and need to be corrected using the C_{heat} factor.

Based on the modeling results, it is possible to estimate the relative importance of heat loss through the system. The mean value of the ratio between Q_c and $Q_c + Q_{out}$ is 10.7%. This small fraction of heat loss through the GDL puts in evidence the importance of the packaging on heat transfer. The fact that dry hydrogen was supplied to the anode using a stoichiometry ratio of 3 has a small impact on the thermal balance since heat loss through heating of the hydrogen supply at the anode is only up to 1.1% of total heat loss of the system and heat generated through condensation of water is less than 0.25%.

4. Investigation of water management problems

4.1. Dry-out

As presented in [13,17], operation of a small PEMFC is divided into three main regions: humidification, flooding, and dry-out. Fig. 4 presents the relative humidity curve of the cathode, which increases up to 100% RH_C at a current density of 65 mA cm^{-2} (humidification). In the second region, relative humidity is saturated at 100%, which means that water is condensing in the cell. Water flux generated through the electrochemical reaction is higher than water flux removed via free convection. At a current density of 320 mA cm^{-2} relative humidity of the cathode begins to decrease with increasing current density. Under these conditions the increase in water partial pressure with current density is not significant enough to compensate for the increase in saturation pressure due to temperature augmentation of the cell.

Moreover, decreasing relative humidity will increase ionic resistance of the electrolyte and lead to a larger voltage drop in the cell. This loss will further raise the fuel cell temperature and accelerate the drop in relative humidity until the cell reaches a limiting current (I_l) caused by an excessively high ionic resistance and the heat generation that will. This third zone is the dry-out of the cell and has been explained by O'Hayre et al. [17].

To better understand the manifestation of flooding and dry-out phenomena, Fig. 4 compares the water flux generated by the

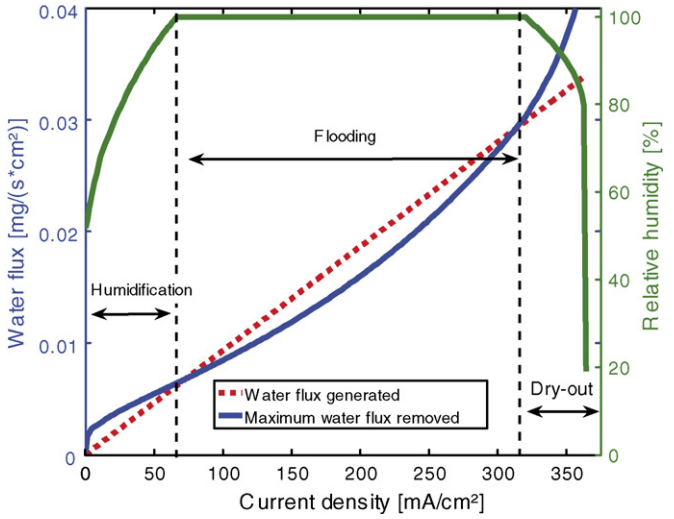

Fig. 4. Reference model results for water flux generated by electrochemical reaction and maximum water flux removed by free convection mass transfer. Relative humidity at the cathode is also plotted as a function of current density. With increasing current density, water balance in the cell changes from humidification, to flooding, and then to dry-out.

electrochemical reaction versus the maximum water flux removed through free convection [17]. The three zones in Fig. 4 are separated by two points of operation under which maximum water removal rate is at the same level as the water generation rate. It should be noted that water removal flux is calculated using the saturated value of water in air. Therefore, this represents the maximum water flux that can be removed from the cell by evaporation. In humidification and dry-out regions, where water flux removal rate at 100% RH is higher than the water flux generated, the water flux removed from the system will decrease in order to match the water flux generated. Under this condition, relative humidity of the cell will drop under 100% as presented in relative humidity curve in Fig. 4. But, in the flooding region, the water flux removed will not be able to match the generated water flux because it is already at its maximum value. Consequently, steady-state operation in this region is not possible without flooding.

The transition points between these zones are dependant on the system configuration and environmental conditions. Electrical resistance, thermal resistance, mass transport resistance, MEA properties, GDL properties, etc. will influence the position and manifestation of these zones of operation. In addition to GDL and MEA properties, packaging of the system will have a strong influence on the PEMFC performance.

4.2. Thermal resistance variation

Let us define the equivalent thermal resistance (R_T) of a small PEMFC as the ratio of temperature difference between the cell and the environment (ΔT) over heat loss from the cell, averaged over all operation points:

$$R_T = \frac{\Delta T}{Q_c + Q_{out}} \tag{33}$$

A system with a higher thermal resistance will have, for the same amount of heat generated by the cell, a higher temperature. With results presented previously, this would mean that increasing the thermal resistance between the PEMFC and its environment would increase the cell's temperature, lower relative humidity and ultimately decrease the limiting current density (I_l) by pushing forward the dry-out problem. This point has already been highlighted by O'Hayre et al. [17] through modeling analysis while considering the effect of GDL thickness. But in a more comprehensive way, this phenomenon not only occurs while changing GDL properties but for the entire packaging of the system. Hence, using the small PEMFC prototype presented previously as a reference, tests were run while changing the thermal resistance of the system to demonstrate this behaviour. Experimental results for the same cell with the surface area and material of the packaging modified to lead to higher and lower thermal resistance are presented in Fig. 5. Ther-

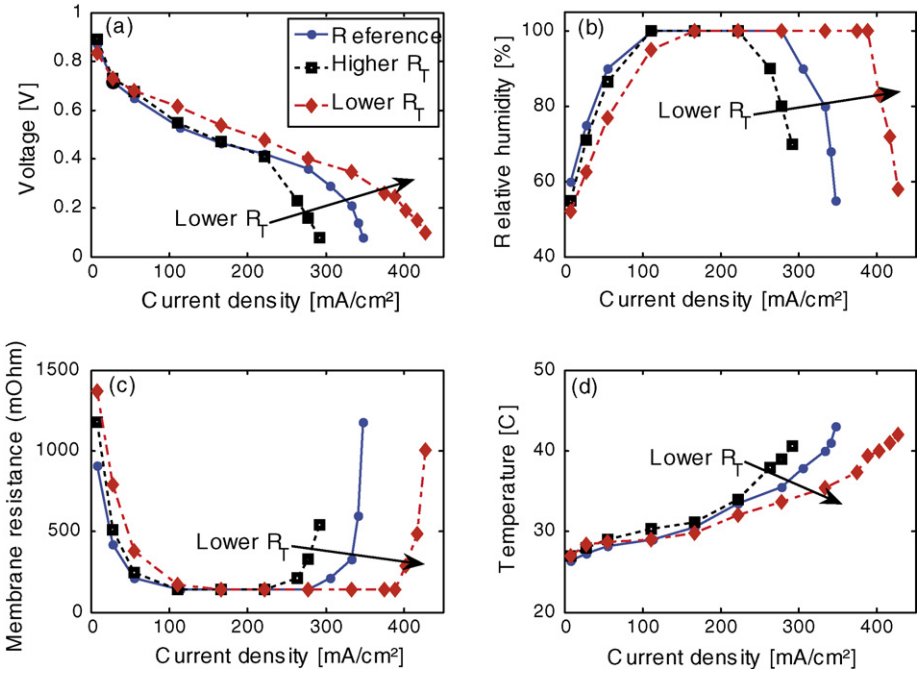

Fig. 5. Experimental results for free convection fuel cell with different thermal resistance values (R_T) as a function of current density, showing that lowering thermal resistance increases limiting current: (a) polarization curves, (b) relative humidity on surface of cathode GDL, (c) fuel cell membrane resistance calculated by Eqs. (23) and (24), based on relative humidity at the surface of the cathode GDL, and (d) temperature on surface of cathode GDL (ambient air at 23.5 °C and 40% RH).

mal resistance is increased by using material with lower thermal conductivity and decreased by adding conductive material to add surface area in contact with the environment.

As shown in Fig. 5 decreasing equivalent thermal resistance increases the limiting current (I_l) and the range in which flooding occurs. The increase in performance is only due to delaying the transition point between the flooding and dry-out regions. With higher thermal resistance, temperature variation as function of current density is higher and the saturation pressure increase is more significant. Thus, the humidity level decreases and the ionic resistance increases are more significant which causes dry-out to occur earlier. This behaviour is pictured by the four curves presented in Fig. 5.

Using the model developed, simulations of cells with various equivalent thermal resistances were carried out to obtain the limiting current density (I_l). Changing thermal resistance in the model slightly affects the mass transport resistance by changing the temperature gradient which affects air properties. Fig. 6 shows that the increase in limiting current density as function of equivalent thermal resistance variation is highly non-linear and increases dramatically around $R_T = 25\,K\,W^{-1}$. As expected from experimental results, lowering thermal resistance increases the limiting current up to a *maximum limiting current density*, $I_{l\text{-max}}$ ($675\,mA\,cm^{-2}$ in Fig. 6). The maximum limiting current density ($I_{l\text{-max}}$) is the current value for which voltage is zero and the limiting water management phenomenon is at the point of transitioning between flooding and dry-out. At this operating point, a small decrease in the equivalent thermal resistance would not allow the system to heat up sufficiently to reach dry-out operation mode before voltage drops to 0 V. Consequently, under these conditions, the limiting factor for the PEMFC would not be dry-out but flooding instead. Limiting current would then be shifted to the transition point between the humidification and flooding zones in Fig. 4 (crossing point furthest to the left). The important point shown in Fig. 6 is that *thermal resistance can significantly increase the limiting current of the cell and control whether the limiting phenomenon is dry-out or flooding*.

4.2.1. Low thermal resistance behaviour

If thermal resistance of the system is low enough, increasing heat loss will not cause the temperature of the cell to rise significantly and consequently the saturation pressure will remain practically constant. Increasing the current density will, however, increase rate of water generated and the water partial pressure. At practically constant temperature, water will eventually accumulate in the system without manifestation of the dry-out phenomenon. Experimentally, this operating mode can be achieved by putting the anode side of the small PEMFC in contact with a large heat sink, such as a massive block of thermally conductive material (stainless steel). This operating mode may seem unusual for a small PEMFC, but in fact it simulates a cell that would be physically integrated into a large system. This effect would be even greater for micro fuel cells.

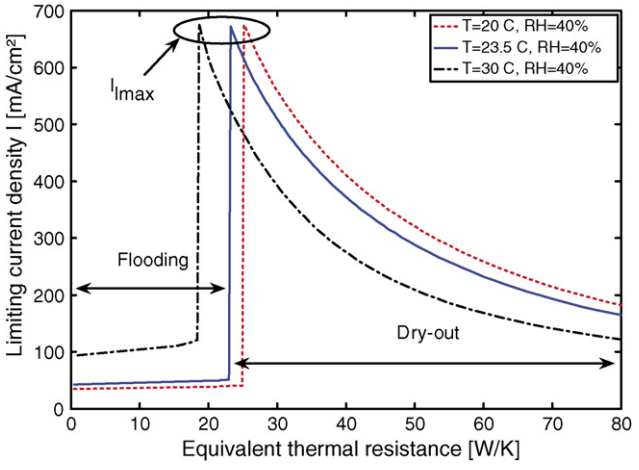

Fig. 6. Model results showing the impact of equivalent thermal resistance (R_T) on the limiting current density for free convection fuel cells. As the R_T is increased, the limiting phenomenon switches from flooding to dry-out (ambient air at 20–30 °C and 40% RH).

The experimental results presented in Fig. 7 show that temperature variation on the surface of the GDL of a small PEMFC in contact with a heat sink is very low; temperature variation is less than 0.5 °C for a current density up to $100\,mA\,cm^{-2}$. Under these operating conditions, the limiting current in steady-state operation is low ($150\,mA\,cm^{-2}$) and occurs because of the formation of water droplets on the surface of the GDL as observed visually; the dry-out phenomenon is never reached. This highlights the importance of thermal rejection on water management problems, which in this case creates a flooding problem instead of a dry-out phenomenon.

4.2.2. Robustness

As shown in Fig. 6, change in environment temperature or relative humidity shifts the limiting current curve and changes the optimal point of equivalent thermal resistance. In order to achieve system robustness, one would have to consider these phenomena and use a more indulgent heat rejection configuration in order to achieve dry-out phenomenon on a larger range of values and avoid flooding as the limiting phenomenon. Otherwise a system designed tightly around an optimum value for a certain environmental condition might not be able to reach steady-state operation in environments of higher relative humidity and/or lower temperature.

4.3. Mass transport resistance variation

Let us define the equivalent mass transport resistance (R_M) of a small PEMFC as the ratio between water partial density variation and water generated by the system, averaged over all operation points:

$$R_M = \frac{\Delta\rho_{H_2O}}{\dot{m}_{H_2O}} \tag{34}$$

As for thermal resistance, mass transport resistance will impact the performance of a small PEMFC running in free convection mode. If system mass transport resistance is increased, the water molar fraction will increase and the oxygen molar fraction at the cathode will decrease. From a water management perspective, this will allow the cell to reach higher current density due to lower water removal rate, which will push forward the transition point between flooding and dry-out. This will be true unless mass transport resistance is too high and creates significant voltage drop due to lack of oxygen. Using the modeling results, we can plot oxygen and water vapour molar fraction against current density.

Fig. 8 shows that the oxygen molar fraction does not decrease significantly, even at high current density. Molar fraction of oxygen varies from 0.21 to 0.14 when current density goes from 0 to $300\,mA\,cm^{-2}$. Also, according to this trend, the model predicts that oxygen molar fraction would reach 0 at about $1600\,mA\,cm^{-2}$, which is quite superior to any results presented here and for any free convection micro-PEMFC. An important conclusion that can be drawn is that oxygen depletion at the cathode catalyst zone, due to pure mass transport problems, is not the actual problem that limits small PEMFC when running in free convection mode. The same conclusion was drawn by Modroukas [15] and O'Hayre et al. [17].

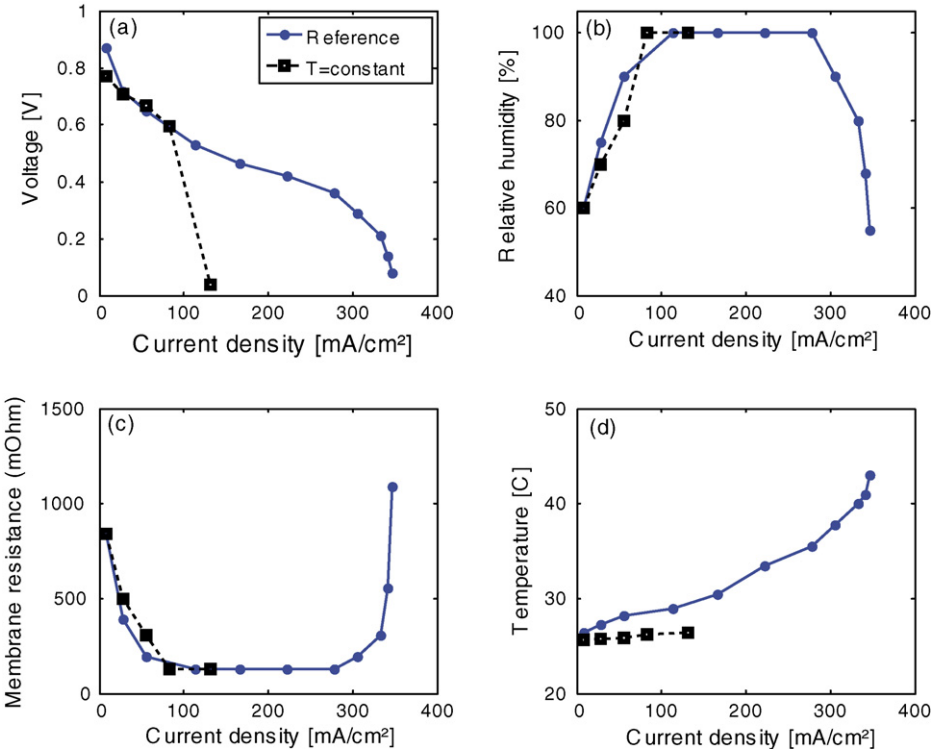

Fig. 7. Experimental results for free convection fuel cell operated with a high thermal resistance and a low thermal resistance (heat sink) that allows practically constant temperature as a function of current density, showing that low thermal resistance system was limited by flooding problems: (a) polarization curves, (b) relative humidity on surface of cathode GDL, (c) fuel cell membrane resistance calculated by Eqs. (23) and (24), based on relative humidity at the surface of the cathode GDL, and (d) temperature on surface of cathode GDL (ambient air at 23.5 °C and 40% RH).

The experimental impact of changing mass transport resistance was evaluated by using as reference the small PEMFC presented previously and by adding a screen on the cathode's GDL top surface. The screen, which consists of a carbon cloth identical to the current GDL, increases the mass transport resistance to and from the cathode. For these tests, temperature and relative humidity were measured at the top surface of the cathode GDL in order to compare with previous results.

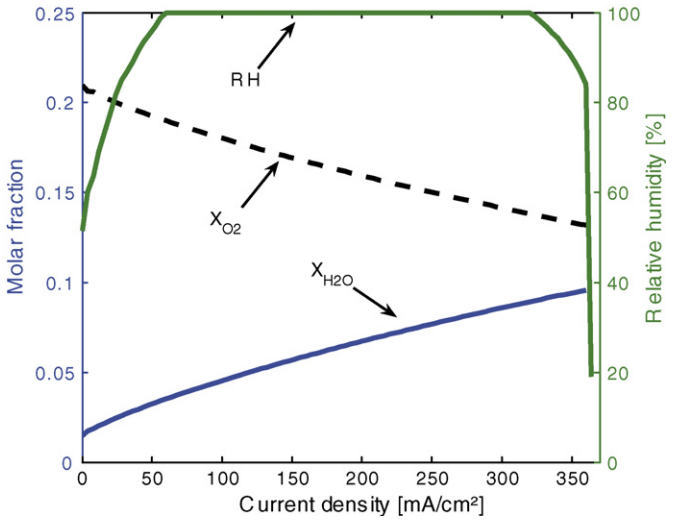

Fig. 8. Reference model results for relative humidity and species molar fraction at the surface of cathode GDL as a function of current density for free convection fuel cell operated at ambient air at 23.5 °C and 40% RH. These results show that oxygen depletion is not the limiting phenomenon, even at higher current densities.

The trends described above are shown experimentally in Fig. 9. Adding mass transport resistance to the system increases maximum limiting current. With a higher mass transport resistance the system will have a higher molar fraction of water at the cathode, so for a same temperature, the water activity in the membrane will be higher. This will prevent dry-out of the electrolyte and increase the limiting current. Fig. 9 shows that at 285 mA cm^{-2}, the relative humidity of the reference test is decreasing while the relative humidity of the prototype with higher mass transport resistance is still saturated at 100%. Up to this point the temperature values for both tests are similar but because of the relative humidity decrease, the reference test temperature starts to increase due to augmentation of ionic resistance that generates more heat loss. Adding a screen on the surface of the GDL increases the thermal resistance, and as presented above, this should decrease the limiting current. But, the increase in mass transport resistance is more significant and performances increase instead of decreasing. This proves that increasing mass transport resistance of a small PEMFC that is nominally limited by dry-out can *increase* its performances by keeping water in the cell. Just as thermal resistance was found to be critical, changing mass transport resistance can also modify the fuel cell performance and impact the water management challenges.

5. Discussion on water management

5.1. Limiting phenomena

Reducing thermal resistance and increasing mass transport resistance allows small air breathing PEMFC to reach higher limiting current densities. This is done by pushing the transition point between flooding and dry-out phenomena to higher current densities. However, the operating range in which flooding occurs

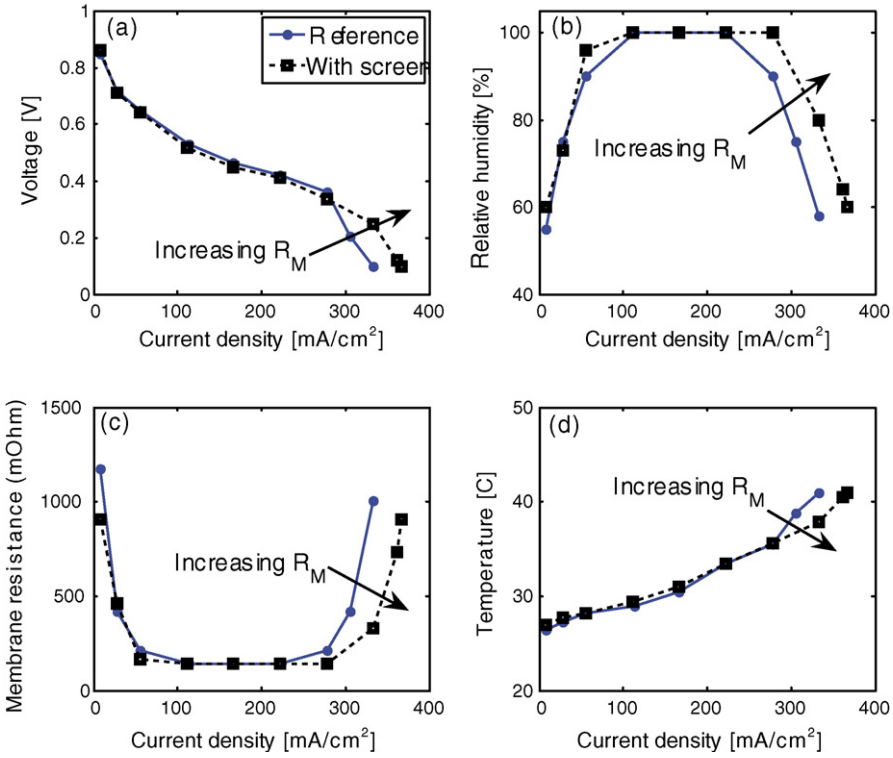

Fig. 9. Experimental results for free convection fuel cell with different mass transport resistance (R_M), showing that increasing mass transport resistance increases the limiting current: (a) polarization curves, (b) relative humidity on surface of cathode GDL as a function of current density, (c) fuel cell membrane resistance calculated by Eqs. (23) and (24), based on relative humidity at the surface of the cathode GDL as a function of current density, and (d) temperature on surface of cathode GDL as a function of current density (ambient air at 23.5 °C and 40% RH).

broadens. Ultimately, with further reduction in thermal resistance, dry-out operating mode will not be reachable and only flooding of the system will be achievable beyond the humidification operating zone. The packaging, through its thermal and mass transport resistance, establishes what kind of limiting phenomena will occur. For example, a small package with high thermal resistance and low mass transport resistance will exhibit the dry-out phenomenon. In the opposite situation, a large package with low thermal resistance and high mass transport resistance can result in flooding problems. This conclusion allows to unify observations from Refs. [14–16] stating that the limiting phenomenon is flooding with conclusions from Refs. [8,13,17] that the limiting phenomenon is dry-out.

However, another point that must be considered regarding the manifestation of limiting phenomena is the *ideal limiting current density* ($I_{l\text{-ideal}}$), which is the limiting current of the system if no mass transport, flooding or dry-out phenomena occur. The limiting current value in this ideal case is solely due to the voltage drop from reaction kinetics and Ohm's law with constant ionic resistance, so this value is fixed by cell properties and electrical resistance of the system. This value will become the limiting phenomenon when the following ratio is respected:

$$\frac{I_{l\text{-ideal}}}{I_l} \leq 1 \tag{35}$$

In this particular case, the limiting current (I_l) due to dry-out or flooding will not be reachable because loss from electrical resistances or reaction kinetics would be too important. In order to get higher performance, one would have too lower these losses instead of working on thermal or mass transport resistance.

5.2. Operating considerations

Using the model, relative humidity for three different thermal resistances was plotted in Fig. 10. Sufficiently low thermal resistance will maintain the flooding operating mode without reaching the dry-out mode, as shown for $R_T = 11.6$ in Fig. 10. This condition

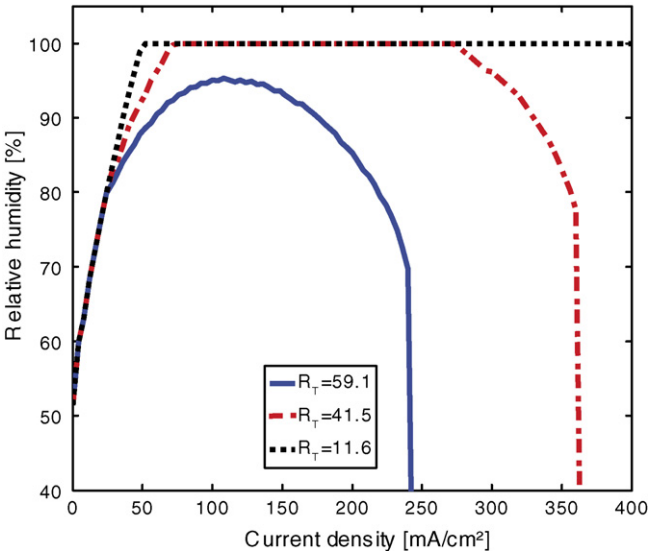

Fig. 10. Model results of relative humidity on surface of cathode GDL as a function of current density for free convection fuel cell. For high equivalent thermal resistance ($R_T = 59.1\ K\,W^{-1}$) there is no flooding zone, only humidification and dry-out occur. For intermediate equivalent thermal resistance ($R_T = 41.5\ K\,W^{-1}$) there are three zones: humidification, flooding and dry-out. For low equivalent thermal resistance ($R_T = 11.6\ K\,W^{-1}$) there is no dry-out zone (ambient air at 23.5 °C and 40% RH).

is possible if temperature variations are kept very low so that the partial pressure of water will remain higher than the saturation pressure value. Under this condition, the transition point between flooding and dry-out operating mode disappears and the limiting current of the system is fixed by the transition between humidification and flooding operating mode. The system could then only be operated in steady-state regime in the humidification zone.

However, if thermal resistance is increased sufficiently, the flooding operating zone will disappear, as presented for the equivalent thermal resistance curve of $R_T = 59.1\ K\,W^{-1}$ in Fig. 10. Maximum water removal rate will always be greater than water generated by the electrochemical reaction. Water flux removed will adjust itself to the water generated and will bring the system down to a relative humidity lower than 100%. Considering the shape of the maximum water removal rate at low current density, relative humidity will first increase without reaching 100% and eventually will decrease. Therefore, only humidification and dry-out operating modes will occur. However, it is important to consider that every operating point will be achievable because there is no flooding zone, which is not the case with the intermediate equivalent thermal resistance curve ($R_T = 41.5\ K\,W^{-1}$). Under this mode of operation, there will be a range in which long-term operation is not possible because of flooding. In order to decrease the flooding zone and increase robustness, the thermal resistance must be increased and/or the mass transport resistance must be decreased. However, increasing robustness of the system is done at the cost of reducing the limiting current density.

5.3. Thermal resistance and mass transport resistance ratio

The previous discussion for water management within free convection fuel cells was mainly conducted considering various thermal resistances but at a constant mass transport resistance. However, as demonstrated similar results can be achieved by changing mass transport resistance and keeping the thermal resistance practically constant. Hence, increasing thermal resistance and/or lowering mass transport resistance reduces the humidity level in the system either by increasing the saturation pressure or lowering the water partial pressure. This favours dry-out as the limiting phenomenon. On the opposite, decreasing thermal resistance and/or increasing mass transport resistance would lead to a flooding problem. Since these resistances variations act in opposite ways, one can define a ratio between thermal and mass transport resistances that would describe which limiting phenomenon will occur. Considering the units of thermal and mass transport resistance, we can define a non-dimensional *water management ratio* of the system (WM_{ratio}) by multiplying the ratio of resistances by the specific heat and density of air:

$$WM_{ratio} = \frac{R_T}{R_M} C_p \rho \tag{36}$$

For the reference prototype presented in this paper, the transition point between dry-out and flooding limitation phenomena would occur at $WM_{ratio} = 0.026$ for a PEMFC operated at ambient air of 23.5 °C and a relative humidity of 40%. It is important to understand that this specific value is valid only for the prototype and its specific geometry.

6. Conclusion

In this paper, we have presented a simple 1D model of a free convection PEMFC that couples heat and mass transfer with the electrochemical reaction of a small PEMFC. Experimental results using a small air breathing PEMFC prototype with a planar configuration validate the consistency of this model. However, simplifications used in the model regarding heat transfer did not allow an exact agreement between experimental and model results, so a correction factor was necessary to get a better match between temperatures. The model would have advantage to be improved regarding heat transfer analysis. Also, the analogy between heat and mass transfer was used to calculate coefficients and each phenomenon was considered separately. The model would be improved if one would merge these two phenomena while evaluating heat and mass transfer coefficients.

Analysis was conducted using the model along with various experimental investigations to evaluate dry-out and flooding phenomena and the impact of thermal resistance and mass transport resistance of a small PEMFC running in free convection mode. Discussion of water management was made regarding limiting phenomena and operation of such a system. Dependency of thermal resistance and mass transport resistance of the system was demonstrated concerning cell performances limitations due to water management problems.

Important conclusions were drawn concerning water management problems for small free convection fuel cells:

(1) The ratio between thermal and mass transport resistance (WM_{ratio}) of the packaging is a critical aspects for water management, controlling if and when dry-out or flooding problems will occur.
(2) High ratio of resistances tends to dry-out the electrolyte, leading to increased ionic resistance and a voltage drop limiting the achievable current density.
(3) Low ratio of resistances could lead to flooding of the cathode that would prevent oxygen mass transport to the catalytic sites and limit the achievable current density. This is characteristic of small and micro fuel cells integrated into larger system.
(4) Fuel cells running in free convection mode are characterized by three modes of operation: humidification, flooding and dry-out, as presented by Refs. [13,17]. The manifestation of these modes is affected by the system's packaging properties and the surrounding conditions.
(5) Considering fuel cells limited by dry-out, there is a compromise between the maximum limiting current density and robustness of the system: the flooding zone will broaden when the maximum current density is increased through a diminution of the ratio between thermal and mass transport resistance.
(6) Mass transport voltage drop caused by a lack of oxygen at the cathode, due to pure mass transport problems and not flooding, is not significant considering the limiting current density of air breathing small PEMFC. The same conclusion was also drawn by Modroukas [15] and O'Hayre et al. [17].

Finally, the conclusions brought by this paper show the impact of packaging for performances reached by a small fuel cell. The importance of heat and mass transfer of an air breathing fuel cell makes the design of the packaging critical for the performance of the system. Thus, further work concerning small PEMFC would benefit from placing emphasis on packaging design. This is even more critical for micro fuel cells which are dominated by heat transfer through the packaging. For low thermal resistance systems emphasis should be placed on removing adequately water in order to increase performance. On the other hand, for high thermal resistance system, emphasis should be placed on increasing thermal rejection and lowering water removal to achieve higher performance [17]. One would need to keep in mind that thermal rejection and mass transport are linked by the free convection phenomena which will push both elements in the same direction. However, it is possible to change more significantly one element. For example mass transport resistance will be more affected than thermal resistance by changes in GDL porosity, while changing the packaging size without changing the cell's active surface or cathode exposed area

will affect the thermal resistance more considerably. The simple modeling approach and non-dimensional water management ratio defined here can guide a designer in developing high performance air breathing fuel cells.

Acknowledgements

The author would like to acknowledge the financial contribution of the Natural Sciences and Engineering Research Council of Canada (NSERC), FQRNT and the Canada Research Chairs program without which this work would not have been possible.

References

[1] H.L. Maynard, J.P. Meyers, J. Vac. Sci. Technol. B 20 (2002) 1287–1297.
[2] J.P. Meyers, H.L. Maynard, J. Power Sources 109 (2002) 76–88.
[3] D. Dunn-Rankin, E.M. Leal, D.C. Walther, Progress Energy Combust. Sci. 31 (2005) 422–465.
[4] C.K. Dyer, J. Power Sources 106 (2002) 31–34.
[5] C. Buie, J.D. Posner, T. Fabian, S. Cha, D. Kim, F.B. Prinz, J.K. Eaton, J.G. Santiago, J. Power Sources 161 (2006) 191–202.
[6] D. Chu, R. Jiang, J. Power Sources 83 (1999) 128–133.
[7] T. Hottinen, M. Noponen, T. Mennola, O. Himanen, M. Mikkola, P. Lund, J. Appl. Electrochem. 33 (2003) 265–271.
[8] S.U. Jeong, E.A. Cho, H. Kim, T. Lim, I. Oh, S.H. Kim, J. Power Sources 158 (2006) 348–353.
[9] P.-W. Li, T. Zhang, Q.-M. Wang, L. Schaefer, M.K. Chyu, J. Power Sources 114 (2003) 63–69.
[10] A. Schmitz, M. Tranitz, S. Eccarius, A. Weil, C. Hebling, J. Power Sources 154 (2006) 437–447.
[11] W. Ying, J. Ke, W. Lee, T. Yang, C. Kim, Int. J. Hydrogen Energy 30 (2005) 1351–1361.
[12] W. Ying, T. Yang, W. Lee, J. Ke, C. Kim, J. Power Sources 145 (2005) 572–581.
[13] T. Fabian, J.D. Posner, R. O'Hayre, S.-W. Cha, J.K. Eaton, F.B. Prinz, J. Power Sources 161 (2006) 168–182.
[14] T. Mennola, M. Noponen, M. Aronniemi, T. Hottinen, M. Mikkola, O. Himanen, J. Appl. Electrochem. 33 (2003) 979–987.
[15] D. Modroukas, Mass Transport Studies in Conventional and Microfabricated Free Convection Proton Exchange Membrane Fuel Cells (2006), Ph.D. thesis, Dept. of Mech. Engg., Columbia University.
[16] D. Modroukas, V. Modi, L.G. Fréchette, J. Micromech. Microeng. 15 (2005) 193–201.
[17] R. O'Hayre, T. Fabian, S. Litster, F.B. Prinz, J.G. Santiago, J. Power Sources 167 (2007) 118–129.
[18] S.O. Morner, S.A. Klein, J. Solar Energy Eng. 123 (2001) 225–231.
[19] R. Chen, T.S. Zhao, J. Power Sources 152 (2005) 122–130.
[20] F.P. Incropera, D.P. Dewitt, Fundamentals of Heat and Mass Transfer, 5th ed., Wiley, New York, 2001, p. 981.
[21] P. Berg, K. Promislow, J. St. Pierre, J. Stumper, B. Wetton, J. Electrochem. Soc. 151 (2004) 341–353.
[22] S. Ge, X. Li, B. Yi, I. Hsing, J. Electrochem. Soc. 152 (2005) 1149–1157.
[23] R.B. Bird, W.E. Stewart, E.N. Lightfoot, Transport Phenomena, 2nd ed., Wiley, New York, 2002, p. 895.
[24] J. Larminie, A. Dicks, Fuel Cell Systems Explained, 2nd ed., Wiley, Chichester, 2003, p. 406.
[25] Y. Sone, P. Ekdunge, D. Simonsson, J. Electrochem. Soc. 143 (1996) 1254–1259.
[26] G.J. Van Wylen, R.E. Sonntag, P. Desrochers, Thermodynamique appliquée, 2ième éd., Éditions du Renouveau pédagogique, Montréal, 1992, p. 781.